PASJ: Publ. Astron. Soc. Japan , 1–??,

Collisional Evolution of Galaxy Clusters and the Growth of Common Halos

Koji Takahashi[1], Tomohiro Sensui[1], Yoko Funato[2],
and
Junichiro Makino[1]
[1]*Department of Astronomy, School of Science, The University of Tokyo, Bunkyo-ku, Tokyo 113-0033*
takahasi@astron.s.u-tokyo.ac.jp
[2]*General Systems Sciences, Graduate Division of International and Interdisciplinary Studies, The University of Tokyo, Meguro-ku, Tokyo 153-8902*

(Received 2001 June 22; accepted 2001 October 11)

Abstract

We investigated the dynamical evolution of clusters of galaxies in virial equilibrium using Fokker–Planck models and self-consistent N-body models. In particular, we focused on the growth of a common halo, which is a cluster-wide halo formed by matter stripped from galaxies, and the development of a central density cusp. The Fokker–Planck models include the effects of two-body gravitational encounters both between galaxies and between galaxies and common halo particles. The effects of tidal mass stripping from the galaxies due to close galaxy–galaxy encounters and accompanying dissipation of the orbital kinetic energies of the galaxies were also taken into account in the Fokker–Planck models. We find that the results of the Fokker–Planck models are in excellent agreement with those of the N-body models regarding the growth of the common halo mass and the evolution of the cluster density profiles. In the central region of the cluster, a shallow density cusp, approximated by $\rho(r) \propto r^{-\alpha}$ ($\alpha \sim 1$), develops. This shallow cusp results from the combined effects of two-body relaxation and tidal stripping. The cusp steepness, α, weakly depends on the relative importance of the tidal stripping. When the effect of stripping is important, the central velocity dispersion decreases as the central density increases and, consequently, a shallow ($\alpha < 2$) cusp is formed. In the limit of no stripping, usual gravothermal core collapse occurs, i.e. the central velocity dispersion increases as the central density increases with a steep ($\alpha > 2$) cusp left. We conclude from our consideration of the origin of the cusp demonstrated here that shallow cusps should develop in real galaxy clusters.

Key words: galaxies: clusters: general — galaxies: evolution — galaxies: interactions — stellar dynamics

1. Introduction

Many observations suggest that clusters of galaxies contain substantial amounts of mass in the form of a background intergalactic stellar component (e.g., Vílchez-Gómez et al. 1994; Scheick, Kuhn 1994; Ferguson et al. 1998 and references therein). It has usually been thought that such a component has its origin in stars stripped from galaxies by galaxy–galaxy encounters, or by the cluster tidal field. However, detailed numerical simulations of galaxy clusters are required to confirm how efficient such mass stripping is and how the structure of the background component evolves.

It was only recently that fully self-consistent N-body simulation of galaxy clusters, with each galaxy represented by many particles, was made possible, because such a full simulation requires huge computing resources. Funato et al. (1993) investigated the evolution of isolated clusters of galaxies using self-consistent N-body simulations. Similar simulations were also performed by Bode et al. (1994) and Garijo et al. (1997). More recently, Sensui et al. (1999, SFM99; 2000, SFM00) followed up the study of Funato et al. (1993) by performing larger N simulations for a wider variety of initial conditions. In their simulations, clusters were initially in virial equilibrium, and all of the cluster mass was initially bound to individual galaxies; a cluster was composed of about 100 identical galaxies, and each galaxy was modeled with 500–4000 particles. SFM99 and SFM00 found that, in all cases, more than half of of the total mass is stripped from galaxies in a few crossing times of the cluster, and that the stripped matter forms a smooth cluster-wide common halo. They also found that a density cusp, approximated as $\rho \propto r^{-\alpha}$ (α being form -1 to -1.5), develops in the central region. However, the physical mechanism of the cusp formation was not clear.

Even if we are allowed to regard clusters of galaxies as "pure" self-gravitating many-body systems composed of point masses (stars and dark matter particles), we have to admit that their evolution is complicated by many phys-

ical processes which take place simultaneously: gravitational encounters, physical collisions, and merging between galaxies; galaxy–background particle interactions, mass stripping from galaxies, internal evolution of galaxies, etc. Therefore, there is no doubt that fully self-consistent N-body simulations are most desirable to obtain qualitatively and quantitatively reliable results on cluster evolution (see García-Gómez et al. 1996).

Nevertheless, more idealized or more simplified models that include (part of) relevant physical processes in approximate ways, such as Fokker–Planck (FP, hereafter) models which we used in the present study, are still very useful regarding two points. First, we can quickly obtain an overview of cluster evolution based on various initial conditions by using approximate models, which are inexpensive in computation time. Second, it is expected that we can understand more clearly the role and importance of each physical process, because we can easily separate the effects of various processes in approximate models. On the other hand, it is often difficult to "understand" the results of N-body simulations, where all processes are automatically included and connected through a complicated procedure. Thus, N-body and approximate models are complementary to each other, and comparison between these models will be particularly helpful to our further understanding of the physics of cluster evolution, regardless of whether agreement or disagreement is found.

Merritt (1983, 1984, 1985) explored the evolution of clusters of galaxies using such approximate models based on an isotropic orbit-averaged FP equation (Cohn 1980). The FP equation describes the evolution of the phase-space distribution function driven by gravitational two-body encounters, and has been applied mainly to globular clusters (see, e.g., Spitzer 1987 for a review). A typical cluster of galaxies is composed of $N = 100$–1000 galaxies, and thus the time scale of two-body relaxation between galaxies, $T_{\rm r}$, is of the same order as the crossing time of the cluster, $T_{\rm cr}$ ($T_{\rm r}/T_{\rm cr} \approx 0.1N/\ln N$). Therefore, two-body relaxation is expected to play an important role in the evolution of galaxy clusters. In his models, Merritt also took account of mass stripping from galaxies due to tidal interactions between galaxies. Since the stripped particles (stars or dark matter particles) were considered to be much lighter than galaxies, these particles were treated as being massless. Dynamical friction between the galaxies and the background massless particles was also included. Thus, in Merritt's models the evolution of the galaxies and the background was treated self-consistently. FP models are continuum models, and therefore have an advantage that they are free from statistical fluctuations, which are unavoidable in N-body models and make it difficult to understand the underlying physics. Yepes et al. (1991) and Yepes and Domínguez-Tenreiro (1992) studied the evolution of galaxy clusters by solving the moment equations of the FP equation. They also included a background component of massless particles in their models, but did not take account of tidal stripping.

The purpose of the present work was to investigate the dynamical evolution of clusters of galaxies after virialization. In particular, we aimed to clarify the physical mechanisms of the growth of the common halo, and of the development of the central density cusp, which were investigated by SFM99 and SFM00 with N-body models. For this purpose, we used FP models, which are based on Merritt's (1983) formulation, but are improved in many aspects, and compare them with the self-consistent N-body models of SFM99 and SFM00. As shown below, the results of the FP and N-body models agree with each other surprisingly well. This suggests that our FP models correctly include all important physical processes, and thus can be used as a useful tool for studying the dynamics of galaxy clusters.

This paper is organized as follows. The basic equations of the FP models are given in section 2. Section 3 describes the initial conditions of our simulations, and section 4 briefly describes the numerical schemes used for our FP and N-body simulations. The simulation results are given in sections 5 and 6; in section 5, the FP and N-body models are compared with respect to the growth of the common halo and the development of the central cusp; in section 6, the physical mechanism of the cusp formation is examined in detail based on FP models. We summarize and discuss our results in section 7.

2. Fokker–Planck Models

In this section, we describe FP models of clusters of galaxies. In FP models, individual galaxies are treated as point particles, except that the effects of tidal stripping are considered. Detailed FP simulations of galaxy clusters were first performed by Merritt (1983). We closely follow his formulation. There are, however, three major differences between his and our models: (1) Merritt used isotropic FP models, but we used anisotropic FP models. (2) We used a new cross-section formula of mass stripping from galaxies based on recent N-body experiments by Funato and Makino (1999, FM). (3) Dissipation of the orbital kinetic energies of galaxies during galaxy–galaxy encounters was also considered, while it was neglected in Merritt's simulations.

2.1. The Fokker–Planck Equation

Consider a self-gravitating many-body system composed of different mass components with particle mass m_i ($i = 0, 1, 2, \ldots$). We write the *number density* in μ-space, i.e. the distribution function, of component m_i as $f_i(\boldsymbol{r}, \boldsymbol{v}, t)$. By assuming that the system is spherically symmetric and in dynamical equilibrium, f_i can be written as a function of the energy per unit mass, E, and the angular momentum per unit mass, J. Then, the orbit-averaged FP equation, under the fixed gravitational potential, can be written as follows (Cohn 1979; Takahashi 1997):

$$A\frac{\partial f_i}{\partial t} = \frac{\partial}{\partial E}\left(D_{Ei}f_i + D_{EEi}\frac{\partial f_i}{\partial E} + D_{ERi}\frac{\partial f_i}{\partial R}\right) + \frac{\partial}{\partial R}\left(D_{Ri}f_i + D_{REi}\frac{\partial f_i}{\partial E} + D_{RRi}\frac{\partial f_i}{\partial R}\right), \quad (1)$$

where R denotes the scaled angular momentum, A is a weight function, and D_{Ei}, D_{EEi}, etc. are flux coefficients. See Takahashi (1997) for a complete description of this equation. To follow the evolution of the system, this FP equation is solved in combination with Poisson's equation (Cohn 1979).

We introduce the *mass density* in phase space,

$$g_i \equiv m_i f_i. \quad (2)$$

Here, we choose the $i=0$ component for representing the background, or a common halo. We can assume that the mass of a background particle (star) is negligible compared to that of a galaxy. However, the mass density of background particles is comparable to that of galaxies. We now take the limit $m_0 \to 0$ while keeping g_0 finite (i.e. $f_0 \to \infty$). In the FP equation (1), component mass m_i appears only in the flux coefficients. In the limit $m_0 \to 0$, the expressions for the first and second-order flux coefficients look like

$$D_{E0} = 0, \quad D_{Ei} \propto m_i \sum_{\text{all } j} g_j \quad (i = 1,2,3,\ldots), \quad (3)$$

$$D_{EEi},\ D_{ERi},\ D_{REi},\ D_{RRi} \propto \sum_{j\neq 0} m_j g_j \quad (i = 0,1,2,\ldots). \quad (4)$$

Note that we write here only the dependence on m_i and g_i symbolically. Exact expressions can be easily obtained from the equations given in the appendix of Takahashi (1997).

The FP equation for the background component ($i=0$) becomes

$$A\frac{\partial g_0}{\partial t} = \frac{\partial}{\partial E}\left(D_{EE0}\frac{\partial g_0}{\partial E} + D_{ER0}\frac{\partial g_0}{\partial R}\right) + \frac{\partial}{\partial R}\left(D_{RE0}\frac{\partial g_0}{\partial E} + D_{RR0}\frac{\partial g_0}{\partial R}\right), \quad (5)$$

which is obtained by multiplying equation (1) by m_0 and then taking the limit $m_0 \to 0$. Since the background particles are massless, they are completely collisionless, i.e., they do not interact with each other. However, galaxies suffer dynamical friction from the background particles that have a finite mass density. Thus, the orbital energy of the galaxies is transferred to the background.

2.2. Mass Stripping Rates

Consider an encounter between *a test galaxy* of mass m and *a field galaxy* of mass m_f, with impact parameter p and relative velocity V. FM showed, both numerically and analytically, that the relative change of the test galaxy's mass in an encounter can be approximated by

$$\frac{\Delta m}{m} = -C'\left(\frac{r_{\rm g}}{p}\right)^{\eta_r}\left(\frac{v_{\rm g}}{V}\right)^{\eta_v}\left(\frac{m_f}{m}\right)^{\eta_m}, \quad (6)$$

with $\eta_r \simeq 2$–3 and $\eta_v \simeq 2$–3, for the cases with $p \gtrsim r_{\rm g}$, $V \gtrsim v_{\rm g}$, and $m = m_f$. Here, C' is a dimensionless constant, and $r_{\rm g}$ and $v_{\rm g}$ are the size (represented by the virial radius in the following) and the three-dimensional internal velocity dispersion of the test galaxy, respectively. Since FM did not carry out simulations of encounters between unequal-mass galaxies, the value of η_m is not determined from their simulations. In the impulse approximation, the velocity change of a star, Δv, is proportional to m_f. Therefore, if the effect of the term $(\Delta v)^2$ is dominant in removing mass from the test galaxy, we may expect $\eta_m \simeq 2$; on the other hand, if the effect of the term $v\Delta v$ is dominant, $\eta_m \simeq 1$ (see Merritt 1983; FM).

Now suppose that a test galaxy experiences successive encounters with field galaxies of mass m_f. The rate of change in the test galaxy's mass is given by

$$\frac{1}{m}\frac{dm}{dt} = n_f \int_{p_{\rm min}}^{p_{\rm max}} 2\pi p dp \int F(\boldsymbol{V}) d^3\boldsymbol{V} V \frac{\Delta m}{m}, \quad (7)$$

where n_f is the number density of the field galaxies and $F(\boldsymbol{V})$ is the (normalized) distribution function of the relative velocity between the test and field galaxies; $p_{\rm min}$ and $p_{\rm max}$ are the minimum and maximum impact parameters, respectively. If we assume a Maxwellian distribution with a three-dimensional velocity dispersion, V_f, for F, this equation becomes

$$\frac{1}{m}\frac{dm}{dt} = -\left(\frac{8\pi}{3}\right)^{1/2} C' n_f r_{\rm g}^2 V_f \left(\frac{v_{\rm g}}{V_f}\right)^{\eta_v}\left(\frac{m_f}{m}\right)^{\eta_m} \int_{x_{\rm min}}^{x_{\rm max}} x^{1-\eta_r} dx \int_0^\infty y^{3-\eta_v}\exp(-y^2/2) dy. \quad (8)$$

Here, we define $x = p/r_{\rm g}$ and $y = \sqrt{3}V/V_f$. The first integral becomes $\ln(x_{\rm max}/x_{\rm min})$ for $\eta_r = 2$, and $1/x_{\rm min} - 1/x_{\rm max}$ for $\eta_r = 3$. Therefore, if we take $p_{\rm min}$ and $p_{\rm max}$ as the size of the galaxy and that of the cluster, we may consider that the integral remains roughly constant during the cluster evolution for $\eta_r = 2$–3. The second integral is also a constant of the order of unity for $\eta_{\rm v} = 2$–3; it equals 1 when $\eta_v = 2$, and $(\pi/2)^{1/2}$ when $\eta_v = 3$.

Therefore, we may rewrite equation (8) as

$$\frac{dm}{dt} = -C\rho_f r_{\rm g}^2 V_f \left(\frac{v_{\rm g}}{V_f}\right)^{\eta_v} \left(\frac{m_f}{m}\right)^{\eta_m - 1}, \tag{9}$$

where C is a dimensionless constant factor and $\rho_f = m_f n_f$ is the mass density of the field galaxies. Note that the definition of C depends on η_r and η_v. When $\eta_v = 2$, for example, $C = (8\pi/3)^{1/2}\ln(p_{\rm max}/p_{\rm min})C'$ for $\eta_r = 2$, and $C = (8\pi/3)^{1/2}(1/p_{\rm min} - 1/p_{\rm max})C'$ for $\eta_r = 3$.

Equation (9) includes two parameters of galaxy's internal structure, $r_{\rm g}$ and $v_{\rm g}$. Because FP models do not follow the internal evolution of galaxies, we have to adopt some relations to express the changes in these parameters by m only. One such relation should be the virial theorem, $v_{\rm g}^2 \propto Gm/r_{\rm g}$. As the other relation we assume $v_{\rm g} \propto m^\zeta$ with $\zeta \simeq 1/4$–$1/3$ (see FM and SFM99). Using these relations we may write the two parameters as

$$\frac{v_{\rm g}}{v_{\rm g0}} = \left(\frac{m}{m_{\rm g0}}\right)^{\zeta}, \quad \frac{r_{\rm g}}{r_{\rm g0}} = \left(\frac{m}{m_{\rm g0}}\right)^{1-2\zeta}. \tag{10}$$

Finally, we obtain

$$\frac{dm}{dt}(r) = -C\left(\frac{r_{\rm g0}^2 v_{\rm g0}^{\eta_v}}{m_{\rm g0}^{2-(4-\eta_v)\zeta}}\right) m^{3-(4-\eta_v)\zeta-\eta_m} \sum_f m_f^{\eta_m - 1}\rho_f(r) V_f^{-(\eta_v - 1)}(r), \tag{11}$$

where a sum over all galaxy components f is taken. We then orbit-average (see, e.g., Takahashi 1997) equation (11) to obtain the mass-loss rate as a function of E and J.

2.3. Energy Dissipation Rates

Stars escape from galaxies via galaxy–galaxy encounters. This is possible because part of the orbital kinetic energies of galaxies is converted into the energy of internal motions of the stars in the galaxies. That is, these encounters are inelastic. If the sum of the galaxy binding energies is much smaller than the cluster binding energy, i.e., if $(v_{\rm g}/V_{\rm cl})^2 \ll 1$ ($V_{\rm cl}$ is the cluster velocity dispersion), the effect of energy dissipation due to inelastic encounters is not very important. However, for our model clusters shown below, this condition is not well satisfied [$(v_{\rm g}/V_{\rm cl})^2 = 5/32$], and therefore energy dissipation is expected to play a non-negligible role.

The binding energy of a galaxy (in virial equilibrium) is $\varepsilon_{\rm g} = mv_{\rm g}^2/2$. The rate of its change is therefore given by

$$\frac{d\ln\varepsilon_{\rm g}}{dt} = \frac{d\ln m}{dt} + \frac{d\ln v_{\rm g}^2}{dt} = (1+2\zeta)\frac{d\ln m}{dt} < 0. \tag{12}$$

Here, in the second equality, we used equation (10). The mass-loss rate is given by equation (11).

The decrease in the binding energy of a galaxy should be compensated by a decrease in the orbital kinetic energies of the galaxies involved in encounters with that galaxy. For simplicity, we assume that the change in the binding energy of a galaxy is just equal to the change in its orbital energy, and that the stripped stars have the same orbital energy per unit mass as that of the parent galaxy. This is valid at least on average. The dissipation rate of the orbital energy of galaxy m is given by

$$m\left(\frac{dE}{dt}\right)_{\rm dis} = \frac{d\varepsilon_{\rm g}}{dt} = (1+2\zeta)\frac{\varepsilon_{\rm g}}{m}\frac{dm}{dt} \tag{13}$$

(remember E represents the energy per units mass). The above assumption ensures that the total energy of a galaxy cluster, including the internal energies of the galaxies, is conserved.

2.4. Implementation of Mass Stripping and Energy Dissipation

The distribution function evolves owing to mass stripping from galaxies as well as owing to two-body relaxation. The effect of mass stripping can be included in the FP equation by adding a source (or sink) term (see, e.g., Quinlan, Shapiro 1989). Thus, in this case the FP equation becomes

$$A\frac{\partial f_i}{\partial t} = \Gamma_i + S_i, \tag{14}$$

where Γ_i denotes the FP collision term [the right-hand side of equation (1)] and S_i represents the source term due to mass stripping. We neglect merging events between galaxies for simplicity. For the initial conditions which we

adopted in this work, N-body simulations showed that mergers were rare (SFM99; SFM00). Therefore, neglect of merging events would not cause serious errors for our models. The source term is calculated in practice as follows.

For each galaxy component i and for each grid point in (E,R) space, we can calculate the change in mass $\Delta m_i(E,R)$ during a time step Δt from the orbit-averaged stripping rate, $\langle dm/dt\rangle_{\rm OA}$. Thus, we know that galaxies of mass $m=m_i$ at time t and position (E,R) will have mass $m'=m_i+\Delta m_i$ $(<m)$ at time $t+\Delta t$, and that each of these galaxies provides mass $m-m'$ for the background. The number of the galaxies does not change during this mass loss, unless they are completely disrupted.

Since we use discrete mass components, a new mass m' is generally not equal to any components m_j, and therefore we have to somehow distribute the galaxies of mass m' among some components. As Lee (1987) and Quinlan and Shapiro (1989) did for stellar mergers in star clusters, we distribute the galaxies by linear interpolation: if n galaxies of mass m' are to be formed and if $m_j \le m' \le m_{j+1}$, then $n(m_{j+1}-m')/(m_{j+1}-m_j)$ galaxies are added to the m_j component and $n(m'-m_j)/(m_{j+1}-m_j)$ galaxies are added to the m_{j+1} component. If $m'<m_1$, where m_1 is a minimum galaxy mass assumed, the galaxies are distributed between $m_0=0$ (background) and m_1. Further we assume that the galaxies after mass stripping and the ejected background particles have the same orbital energy and angular momentum per unit mass (E,R) as the galaxies had before stripping. The effect of energy dissipation is considered separately, as described below.

By doing the above procedure over all of the galaxy components at each grid point in (E,R) space, we can calculate the change in the distribution function due to mass stripping, i.e., the source term, S_i. Note that this procedure guarantees conservation of the total mass and energy of the cluster.

Merritt (1983) formulated mass stripping as a first-order "mass diffusion" term in the FP equation [see his equation (22)]. In his formulation he assumed a distribution function, $f(E,m,t)$, which is continuous with respect to m as well as E. In integrating the FP equation numerically, he used, of course, discrete mass grids. On the other hand, we have assumed discrete mass components from the beginning. Although Merritt's formulation and our formulation may look different apparently, they both consider only the first-order term $\langle\Delta m\rangle$ and are essentially the same.

The effect of energy dissipation (cooling) is included in the FP equation in the same way as the effect of binary heating in star clusters (see, e.g., Takahashi 1997). That is, the cooling term, which may be calculated from equation (13), is added to the first-order energy coefficient, D_E. In practice, the amount of energy dissipation during Δt is calculated so that it should be consistent with the above-described way of distributing stripped galaxies among mass components.

2.5. Time Scales

A commonly used definition of the two-body relaxation time is given by Spitzer (1987, equation [2-61]) as $t_{\rm r}\equiv (v_{\rm m}^2/3)/\langle(\Delta v_\parallel)^2\rangle_{v=v_{\rm m}}$. Here, a Maxwellian velocity distribution of field particles is assumed and $v_{\rm m}^2$ is the three-dimensional velocity dispersion; $\langle(\Delta v_\parallel)^2\rangle_{v=v_{\rm m}}$ is the mean square value of the change per unit time in the velocity component parallel to the initial velocity of a test particle, evaluated at $v=v_{\rm m}$. For the present cases, assuming that all galaxy components follow Maxwellian velocity distributions with the same velocity dispersion, $V_{\rm cl}$, we obtain

$$T_{\rm r}=\frac{0.065V_{\rm cl}^3}{G^2\ln\Lambda\sum_f m_f\rho_f}=\frac{0.065}{G^2\ln\Lambda}\frac{V_{\rm cl}^3}{\langle m_f\rangle_\rho\rho_{\rm gal}}, \tag{15}$$

where $\rho_{\rm gal}=\sum\rho_f$ is the total density of the galaxies and $\langle m_f\rangle_\rho=\sum m_f\rho_f/\rho_{\rm gal}$ is the *mass-weighted* mean galaxy mass. Equation (15) represents the time scale of the velocity diffusion due to encounters between galaxies. Similarly, we define the dynamical friction time as $t_{\rm df}\equiv|v_{\rm m}/\langle\Delta v_\parallel\rangle_{v=v_{\rm m}}|$, where $\langle\Delta v_\parallel\rangle_{v=v_{\rm m}}$ is the mean change per unit time in the velocity component parallel to the initial velocity, evaluated at $v=v_{\rm m}$. On the same assumptions as used in deriving equation (15), we find that the dynamical friction time for a galaxy of mass m is given by

$$T_{\rm df}=\frac{0.13V_{\rm cl}^3}{G^2\ln\Lambda\sum_f (m+m_f)\rho_f}=\frac{0.13}{G^2\ln\Lambda}\frac{V_{\rm cl}^3}{\langle m_f\rangle_\rho\rho_{\rm gal}+m\rho_{\rm tot}}, \tag{16}$$

where $\rho_{\rm tot}$ is the total density including both the galaxy and halo components. Unlike the relaxation time (15), the dynamical friction time (16) depends on the test-particle mass and on the halo density. From equations (15) and (16), it follows that

$$\frac{T_{\rm r}}{T_{\rm df}}=0.5\left(1+\frac{m}{\langle m_f\rangle_\rho}\frac{\rho_{\rm tot}}{\rho_{\rm gal}}\right). \tag{17}$$

In single-component clusters, $T_{\rm r}=T_{\rm df}$. In multicomponent clusters, $T_{\rm df}$ can be much smaller than $T_{\rm r}$ for massive galaxies; this holds also for light galaxies, if $\rho_{\rm tot}\gg\rho_{\rm gal}$.

We define the tidal mass stripping time as $t_{\rm ts} \equiv |m/(dm/dt)|$. Using equation (11) with V_f^2 set equal to $2V_{\rm cl}^2$, we find

$$T_{\rm ts} = \frac{m_{\rm g0}^{2-(4-\eta_v)\zeta}}{C r_{\rm g0}^2 v_{\rm g0}^{\eta_v}} \frac{m^{\eta_m-2+(4-\eta_v)\zeta} (\sqrt{2}V_{\rm cl})^{\eta_v-1}}{\langle m_f^{\eta_m-1}\rangle_\rho \rho_{\rm gal}}. \tag{18}$$

Using equations (16) and (18), with $r_{\rm g0} = G m_{\rm g0}/2v_{\rm g0}^2$, we obtain

$$\frac{T_{\rm ts}}{T_{\rm df}} = \frac{31\ln\Lambda}{C} 2^{(\eta_v-1)/2} \left(\frac{m}{m_{\rm g0}}\right)^{(4-\eta_v)\zeta} \left(\frac{v_{\rm g0}}{V_{\rm cl}}\right)^{4-\eta_v} \frac{\langle m_f\rangle_\rho \rho_{\rm gal} + m\rho_{\rm tot}}{m^{2-\eta_m}\langle m_f^{\eta_m-1}\rangle_\rho \rho_{\rm gal}}. \tag{19}$$

For our standard set of parameters, $\eta_m = 2$, $\eta_v = 2$, and $\zeta = 1/4$ (see section 5), it follows that

$$\frac{T_{\rm ts}}{T_{\rm df}} = 1.8\ln\Lambda \left(\frac{25}{C}\right) \left(\frac{m}{m_{\rm g0}}\right)^{1/2} \left(\frac{v_{\rm g0}}{V_{\rm cl}}\right)^2 \left(1 + \frac{m}{\langle m_f\rangle_\rho} \frac{\rho_{\rm tot}}{\rho_{\rm gal}}\right). \tag{20}$$

This indicates that $T_{\rm ts} \approx T_{\rm df}$ in our initial models (see section 3). As the fraction of the common halo increases, tidal stripping becomes less important (Merritt 1983).

3. Initial Conditions

We use the same initial cluster model as that in SFM99. That is, the initial model is a Plummer model composed of $N_{\rm g} = 128$ identical galaxies with no common halo. Exceptions are models FPA1 and FPA2, which we describe later. The initial galaxy model is also given by a Plummer model as in SFM99. The ratio of the virial radius of each galaxy $r_{\rm vr}$ to the virial radius of the cluster $R_{\rm vr}$ is set equal to 1/20.

Note that initial galaxy models affect FP models only through the mass-stripping rate, equation (11). This equation includes two parameters of the internal structure of galaxies, $r_{\rm g0}$ and $v_{\rm g0}$, but these are related by the virial theorem (we take $r_{\rm g} = r_{\rm vr}$) for a given galaxy's mass. Hence, in FP models the structure of galaxies is represented by only one parameter, e.g., $r_{\rm vr}$. In reality, even if the virial radii are the same, different galaxy models will give different stripping rates. Such differences in galaxy models could be reflected in FP models only by adjusting an undetermined numerical constant, C, in equation (11).

We use a system of units in which $G = 1$, $m_{\rm g} = 1$, and $\varepsilon_{\rm g} = 1/4$, where G is the gravitational constant (Heggie, Mathieu 1986); hence $r_{\rm vr} = G m_{\rm g}^2/(4\varepsilon_{\rm g}) = 1$. For the cluster, we have $M_{\rm cl} = 128$, $R_{\rm vr} = 20$, and $\mathcal{E}_{\rm cl} = 204.8$, where $M_{\rm cl}$, $R_{\rm vr}$, and $\mathcal{E}_{\rm cl}$ are the mass, virial radius, and binding energy of the cluster, respectively. The mean velocity dispersion of stars in a galaxy is $v_{\rm g} = 1/\sqrt{2}$, and that of galaxies in the cluster is $V_{\rm cl} = 4/\sqrt{5}$. The cluster crossing time is

$$T_{\rm cr} = \frac{2R_{\rm vr}}{V_{\rm cl}} = 10\sqrt{5} \simeq 22, \tag{21}$$

and the half-mass relaxation time (Spitzer 1987, equation [2-63]) is

$$T_{\rm rh} = 0.138 \frac{N}{\ln\Lambda} \left(\frac{R_{\rm h}^3}{G M_{\rm cl}}\right)^{1/2} \simeq 19, \tag{22}$$

where the cluster half-mass radius $R_{\rm h} = 15.4$ and the Coulomb logarithm $\ln\Lambda = \ln N = \ln 128$. If we assume that $m_{\rm g} = 10^{12} M_\odot$ and $r_{\rm vr} = 30$ kpc, the cluster model has $M_{\rm cl} = 1.28 \times 10^{14} M_\odot$, $R_{\rm vr} = 0.6$ Mpc, $T_{\rm cr} = 2.5$ Gyr, and $T_{\rm rh} = 2.1$ Gyr.

Only models FPA1 and FPA2 have a common halo initially (see subsection 5.1); the ratio of the common halo mass to the total mass, $M_{\rm h}/M_{\rm cl}$, is 1/2 and 3/4, or if the mass is converted into the number of galaxies, $N_{\rm g} = 64$ and 32, for FPA1 and FPA2, respectively. Galaxy and common halo components are distributed in space so that the ratio of their densities is independent of the radius. The other conditions are the same as those of the other models.

4. Simulations

4.1. Fokker–Planck Simulations

Details of the numerical integration scheme of the FP equation have been described by Takahashi (1995, 1997). We used 301 energy, 51 angular momentum, and 121 radial grid points. We used $K = 20$ mass components for galaxies. These components are uniformly spaced in m between 0 and 1; $m_1 = 1/K$, $m_2 = 2/K$, ..., $m_K = 1$. In addition, one component of $m_0 = 0$ was assigned to a background (common halo). We confirmed that these numbers of grid points and mass components are large enough to obtain satisfactory convergence of the results. The relative errors in the total mass were less than 0.1% and those in the total energy were less than 0.5% in all runs.

We calculated a number of FP models, switching on and off mass stripping and energy dissipation and changing the parameters of the stripping rate. These models are summarized in table 1.

4.2. N-body Simulations

We compared our FP models with the N-body models of SFM99 and SFM00 for the same initial conditions. SFM99 performed a number of simulations for the same initial theoretical model using different random realizations of the model and varying the number of particles for representing each galaxy; they confirmed that the results of those simulations were almost the same. In section 5, the model PP of SFM00, denoted by NB in this paper, is compared with the FP models. The simulation was carried out using GRAPE-4 (Makino et al. 1997) with the Barnes–Hut tree algorithm (Barnes, Hut 1986; Makino 1991; Athanassoula et al. 1998). Each initial galaxy model was represented by 2048 particles, and thus the total number of particles was 262144. For more details of the numerical integration and for a galaxy identification scheme, see SFM99 and SFM00.

5. Comparison between Fokker–Planck and *N*-body Models

5.1. Models with Common Halos but without Mass Stripping

First we discuss the evolution of model clusters in which mass stripping from galaxies is not allowed, but which initially have massive common halos, in order to reveal how such multicomponent systems evolve owing to two-body relaxation only.

Although collisional evolution of multicomponent stellar systems has been investigated by many authors using FP models in the context of globular cluster evolution (e.g., Inagaki, Wiyanto 1984; Cohn 1985; Chernoff, Weinberg 1990; Takahashi 1997 and references therein), massless particle components were not considered in those studies. On the other hand, it is not very difficult to extrapolate the behavior of massless particles from the behavior of particles whose masses are much smaller than the mean particle mass. In that sense, no essentially new results were found in our simulations, as discussed below. However, it is useful to see first how "pure" collisional systems evolve before considering more complicated systems with mass stripping. Yepes et al. (1991) and Yepes and Domínguez-Tenreiro (1992) also studied pure collisional evolution of galaxy clusters including massless particles, but using the moment equations of the FP equation.

Figure 1a shows the evolution of density profiles for model FPA1; the solid lines and dotted lines represent the galaxy and common halo components, respectively. Figure 1b shows the corresponding profiles of the logarithmic gradient defined by

$$\alpha_i \equiv -\frac{d\ln\rho_i}{d\ln r}. \tag{23}$$

Figures 1c and 1d are for model FPA2.

We have assumed that the number of galaxies, $N_{\rm g}$, is 64 and 32 for FPA1 and FPA2, respectively. However, it should be noted that $N_{\rm g}$ is only concerned with time scaling; if time is measured in units of the relaxation time, the evolution of these models does not depend on the number of galaxies, because only the two-body relaxation process is taken into account in them. We set the Coulomb logarithm equal to $\ln(M_{\rm cl}/m_{\rm g}) = \ln 128$ for time scaling for both models.

As is well known, energy redistribution among particles due to two-body relaxation eventually leads the cluster core to gravothermal core collapse (Lynden-Bell, Wood 1968; Lynden-Bell, Eggleton 1980); after the onset of core collapse the central density continues to increase and the core radius continues to decrease, unless other physical mechanisms intervene. Late core collapse proceeds self-similarly with the development of the power-law density cusp, $\rho \propto r^{-\alpha}$. Cohn (1980) found $\alpha = 2.23$ for single-component clusters. In multicomponent clusters, the most massive component eventually dominates the central part, i.e., strong mass segregation occurs, owing to a tendency toward equipartition of energy. Thereafter, the most massive component collapses as in single-component clusters and lighter components have shallower density cusps (e.g., Inagaki, Wiyanto 1984; Chernoff, Weinberg 1990).

The development of the density cusps of the galaxy and common-halo components through gravothermal core collapse is clearly shown in figure 1. Power-law cusps appear for $r \lesssim 1 = R_{\rm vr}/20$. The slopes of the cusps hardly depend on the difference in the initial conditions of FPA1 and FPA2; the slope of the galaxy cusp approaches $\alpha = 2.23$ and the slope of the common-halo cusp is much shallower, $\alpha \sim 0.5$, as expected.

Cohn (1985; see also Chernoff, Weinberg 1990) found that in deep collapse phases of multimass clusters, the power-law indices α_i of the density profiles of different components are approximately related by

$$\alpha_i = 0.23\left(8.2\frac{m_i}{m_{\rm u}} + \frac{3}{2}\right), \tag{24}$$

where $m_{\rm u}$ is the particle mass of the most massive component, which dominates the central potential well. This equation is obtained on the assumption that the distribution function of component i is given by $f_i \propto (-E)^{p_i}$ with

$p_i/p_{\rm u} = m_i/m_{\rm u}$. This relation for $p_{\rm i}$ was originally found by Bahcall and Wolf (1977) for a steady state solution of the stellar distribution around a central massive black hole. In deriving equation (24) the results of numerical simulation (Cohn 1980), $\alpha_{\rm u} = 2.23$ and $p_{\rm u} = 8.2$, are also used.

Equation (24) gives $\alpha_i \to 0.345$ as $m_i \to 0$. Figures 1b and 1d show that the actual slope of the common halo cusp is slightly larger than this predicted value. Such deviation from equation (24) at small masses was also reported by Chernoff and Weinberg (1990).

For models FPA1 and FPA2, we followed the cluster evolution up to a rather deep collapse phase in order to see self-similar development of the density cusps. However, we should keep in mind that it is very unlikely that actual galaxy clusters can reach such deep collapse, because galaxies have appreciable finite sizes compared to the cluster sizes. For our model cluster, the sizes of the galaxies are ~ 1, and thus the core radius of the cluster cannot be less than ~ 1.

5.2. Models with Mass Stripping but without Energy Dissipation

In this section we show the results of FP models in which mass stripping is included but energy dissipation is neglected, and compare these results with N-body results.

Figure 2a shows the fraction of the common halo mass to the total mass as a function of time for models FPB1 and NB. Figure 2b shows the evolution of the central density of the galaxies and that of the common halo, $\rho_{\rm g}(0)$ and $\rho_{\rm h}(0)$. For the N-body model the galaxy density is not plotted, because it changes very noisily with time owing to the small number of galaxies (see figure 6). The center of the cluster of the N-body model was chosen to be the density center (Casertano, Hut 1985) of the common halo particles.

Concerning the growth of the common halo mass, $M_{\rm h}$, the agreement between FPB1 and NB is pretty good, though the growth speed slows down somewhat earlier in FPB1 than in NB. Actually, the value of the numerical constant, $C = 25$, in equation (11) for FPB1 was chosen to achieve such a good agreement. The initial growth rate of $M_{\rm h}$ in the FP model is determined by only the stripping rate for given initial conditions. This means that we can always adjust C to obtain a desirable initial growth rate. Once its value is chosen, however, we have no freedom to adjust later growth of the common halo, which depends on evolving cluster properties. Therefore, the fine tuning of C is not responsible for the overall good agreement observed in figure 2a.

In principle, the value of C can be determined from the data of N-body experiments of galaxy–galaxy encounters such as given by FM. However, its exact value depends on the detailed structure of the galaxies, which changes with time under the cluster environment. From equations (8) and (9), we find, for $\eta_v = 2$, $C' = C(8\pi/3)^{-1/2}/\ln(R_{\rm vr}/r_{\rm vr}) = 0.115C$ if $\eta_r = 2$, and $C' = C(8\pi/3)^{-1/2}/(1/r_{\rm vr} - 1/R_{\rm vr}) = 0.364C$ if $\eta_r = 3$. Hence $C = 25$ corresponds to $C' = 2.9$ and 9.1 for $\eta_r = 2$ and 3, respectively. Equation (6) with these values of C' is consistent, in order of magnitude, with the data of FM (see their figures 7, 8, 11, and 12).

Models FPB1 and NB are in rather good agreement in the evolution of $M_{\rm h}$, but show a clear difference in $\rho_{\rm h}(0)$ evolution: the central density increases much more slowly in FPB1 than in NB. We will see below that the inclusion of energy dissipation, which makes the treatment of tidal stripping in FP models fully self-consistent, removes this difference.

The initial quick increase in $\rho_{\rm h}(0)$ and the initial decrease in $\rho_{\rm g}(0)$ are simply due to the fact that mass stripping from the galaxies suddenly starts at $t = 0$. After a few cluster crossing times, the central galaxy density begins to increase. Mass stripping works only to decrease the galaxy density by removing part of galaxy mass to the common halo. Therefore, the increase in the galaxy density should be due to two-body relaxation. Since the processes of core collapse and mass stripping occur simultaneously, the central density of the galaxies and that of the common halo stay comparable for a long time, while the central density is soon dominated by galaxies in models FPA1 and FPA2 where there is no mass stripping. Figure 2b shows that the galaxy density finally exceeds the common halo density at the center even with mass stripping. We discuss in more detail the process of core collapse with mass stripping in section 6.

Here, we mention the choice of the value of the Coulomb logarithm. As noted above, the central density increase in model FPB1 is significantly slower than that in model NB. We found that rough agreement in the central density evolution was obtained when we artificially increased the two-body relaxation rate by about a factor of two without changing the mass stripping rate. Increasing the relaxation rate by a factor of two is equivalent to doubling the Coulomb logarithm, $\ln\Lambda$, i.e., replacing $\ln 128$ with $2\ln 128 = \ln 128^2$ in the present case. There is some uncertainty for the choice of the exact value of Λ, but it is very unlikely that such a large value as $\Lambda = 128^2$ is justified.

5.3. Models with Mass Stripping and Energy Dissipation

We now take account of the effects of both mass stripping and energy dissipation in FP models (sequence FPC in table 1). The evolution of model FPC1 (our standard model) is shown in figure 3. The growth of $M_{\rm h}$ in FPC1 is similar to that in FPB1, although the former shows a slightly larger growth rate at late epochs. The difference between FPB1 and FPC1 is clear in the evolution of the central density, which increases more rapidly in FPC1 than in FPB1. We now see good agreement between models FPC1 and NB in the central density evolution as well as in the

evolution of the common halo mass. It should be recalled that energy dissipation is included consistently with mass stripping, without introducing any additional free parameters.

In the following, we investigate how sensitively the behavior of FP models depends on the parameters of the mass stripping rate (C, η_v, η_m, and ζ). The probable ranges of these parameters are limited by the results of N-body experiments and theoretical considerations (see section 2.2).

In figure 4 we compare models FPC1, FPC2, and FPC3, which differ only in the value of C ($C = 25$, 15, 35). Larger C gives a higher stripping rate, and consequently faster growth in the mass of the common halo. At early epochs the central density of the common halo also increases more quickly for larger C, but at late epochs it increases more slowly because faster mass stripping prevents the density increase more severely. We conclude that the value of $C = 25$ gives the best agreement between the FP and N-body results.

Figure 5 compares models FPC1, FPC4, FPC5, and FPC6, which differ in the value of η_v, η_m, or ζ (see table 1). For model FPC4 it is necessary to adjust the value of C so that the initial growth rate of the common halo becomes similar to those of the other models. These models are not very different from one another. Therefore, we conclude that the results of FP simulations do not very sensitively depend on the mass-stripping formula as long as the parameters are in reasonable ranges.

One noticeable difference is seen in the evolution of the central density of model FPC5 ($\eta_m = 1$); at late epochs the central density increases more slowly compared with the other models. We find that this is because massive galaxies are much more depleted in model FPC5. In all models, the mean galaxy mass $\langle m_f \rangle_\rho$ in the central regions first decreases quickly and then stays roughly constant as the galaxy density increases. At late epochs, $\langle m_f \rangle_\rho \sim 0.2$ at the center for model FPC5 and ~ 0.4 for the others. This implies that the collapse rate of FPC5 is smaller by about a factor of two. Equation (18) tells us why such a difference occurs; tidal stripping time $T_{\rm ts}$ is proportional to $1/\langle m_f \rangle_\rho$ for $\eta_m = 2$, but $T_{\rm ts}$ does not depend on $\langle m_f \rangle_\rho$ for $\eta_m = 1$. Therefore, while $T_{\rm ts}$ increases as $\langle m_f \rangle_\rho$ decreases in the $\eta_m = 2$ models, it stays almost constant (actually somewhat decreases) in model FPC5. Consequently, $\langle m_f \rangle_\rho$ decreases to a much lower value in FPC5. A comparison with the N-body model in figure 5b supports $\eta_m = 2$ rather than $\eta_m = 1$.

Figure 6 shows the mass-density profiles of models NB (left) and FPC1 (right) at selected epochs. The density profiles for the galaxies (middle) and the common halo (bottom) are plotted separately as well as the total density (top). For model NB, the density profiles of the galaxies are rather noisy because of the small number of galaxies. We should note that a comparison of the profiles of the N-body and FP models on a length scale of $\lesssim 1$ is, at least for the galaxies, meaningless, since the sizes of the galaxies, $r_{\rm g}$, is ~ 1. Thus, for $r \lesssim 1$ in the N-body model, we see the internal structure of a galaxy if any galaxy is there, and a void if not. At late epochs, the central region of the cluster is usually occupied by a few massive galaxies that have sunk there owing to dynamical friction. For $r \gtrsim 1$, models NB and FPC1 show very similar evolution of the density profiles, apart from fluctuations in the N-body model.

The similarity between the two models is more clearly shown in figure 7, which directly compares their density profiles at $t = 8.9\,T_{\rm cr}$. In particular, almost perfect agreement is seen in the density profile of the common halo.

The agreement between the FP and N-body results shown above is enough to convince us that our FP models include all essential physical processes concerned and can describe the cluster evolution rather accurately.

In figure 8 we show the logarithmic density gradient, α [see equation (23)], as a function of the radius for model FPC1 at $t = 8.9\,T_{\rm cr}$, together with the density profiles of FPC1 and NB again. For $1 \lesssim r \lesssim 5$, the value of α for the total density varies gently with the radius from ~ 0.5 to ~ 1.5 with a median value of ~ 1. This implies that the total density profile in this region may be reasonably approximated by a power law, r^{-1}, as SFM99 claimed.

The common halo component dominates the density for $1 \lesssim r \lesssim 20$. For $r \lesssim 1$, the density of the galaxy component overwhelms that of the halo component in the N-body model, while they are comparable in model FPC1. As noted above, this difference arises because in the N-body model a massive galaxy stays around the cluster center at late epochs and its internal structure is observed on this length scale. In fact, the density of the particles in each galaxy is much larger than the density of the common halo particles for $r \lesssim 1$ in NB. This extra density increase in the N-body model strengthens our impression that the total density profile is given by a power law.

It is not clear from figure 8 whether the central density distribution is really described by any single power law, since the central density has not yet increased sufficiently from the initial value. In principle, FP calculations can be (formally) continued further, if we neglect the fact that the galaxies have finite sizes. However, we could actually not continue FP calculations to very advanced stages of core collapse for model FPC1 and other similar models, unlike the case for the models without stripping, owing to numerical instability. This difficulty of FP calculations is linked to the divergence of the distribution function at the center caused by continuous decrease in the central velocity dispersion; see section 6.

In order to see the mass dependence of the galaxy distributions, we divided the galaxies into four mass groups, $m \in (0, 0.25]$, $(0.25, 0.50]$, $(0.50, 0.75]$, and $(0.75, 1]$, and plotted the density profile for each group for model FPC1 at $t = 8.9\,T_{\rm cr}$ in figure 9. It is apparent that heavy galaxies are strongly depleted in the central regions, owing to tidal stripping, and have a very flat density profile. If there were no stripping, the heavy galaxies would dominate the central regions as the result of two-body relaxation.

The development of "inverse mass segregation" is clearly shown in figure 10, which plots the mass-weighted mean galaxy mass, $\langle m \rangle_\rho$, as a function of the radius for model FPC1. The mean mass decreases toward the center. This indicates that mass stripping is more efficient than dynamical friction for heavy galaxies. Only at very late epochs ($t \gtrsim 8.9\,T_{\rm cr}$), when the central density of the galaxies has increased sufficiently high, is a slight increase in the mean mass seen at the center. Similar inverse mass segregation was already found by Funato et al. (1993) and SFM99 in N-body simulations and by Merritt (1984) in FP simulations.

The density profiles of models FPC1–C6 are similar, if they are compared at epochs with the same central density. In particular, the halo density profiles are almost indistinguishable. However, we show in the next section that the density cusp gradient does depend on the stripping rate. It is obvious that the gradient, α, should be close to 2.2 when mass stripping is almost negligible compared to two-body relaxation. On the other hand, if stripping is infinitely fast, all galaxies will dissolve instantaneously and no further evolution of the cluster can occur based on our present assumptions. The stripping rates for models FPC1–C6 are not very different (see figures 4 and 5), and hence the difference in their density profiles is insignificant.

6. Cool Core Collapse and Shallow Density Cusps

In subsection 5.3 we showed that a shallow density cusp, approximated by $\rho \propto r^{-1}$, develops in the central regions of a galaxy cluster. Now let us assume that a collapsing core leaves behind a cusp that exactly follows a power-law, $\rho \propto r^{-\alpha}$. This implies that the central density grows as $\rho_{\rm c}(t) \propto r_{\rm c}^{-\alpha}(t)$, as the core radius $r_{\rm c}(t)$ decreases with time. Similarly, a dimensional analysis implies that the central velocity dispersion changes as $v_{\rm c}^2(t) \propto G\rho_{\rm c} r_{\rm c}^3 / r_{\rm c} \propto r_{\rm c}^{2-\alpha}(t)$ (but this is valid only for $\alpha > 1$ as we discuss later). This relation predicts that the central velocity dispersion increases (i.e. the core gets hotter) as the core shrinks if $\alpha > 2$, and that it decreases (i.e. the core gets cooler) if $\alpha < 2$. For core collapse in star clusters, detailed numerical calculations (Cohn 1980; Lynden-Bell, Eggleton 1980) show that $\alpha = 2.2 > 2$, and that actually both the central density and velocity dispersion increase as the core shrinks — "hot collapse" occurs. For core collapse in galaxy clusters, our calculations indicate $\alpha < 2$. Therefore, we expect "cool collapse" in this case.

Lynden-Bell and Eggleton (1980) proved that α should be in the range $2 < \alpha < 2.5$ for the existence of any self-similar collapse solution in equal-mass clusters. The condition $\alpha > 2$ comes from the requirement that temperature must decrease outward so that the core can shrink by losing heat to the halo. In multimass clusters, however, heat is also transferred among different mass components. Therefore, it can happen that the core of heavy particles loses energy to light particles and shrinks even if $\alpha < 2$.

Let us see in more detail the case of a shallow density cusp,

$$\rho(r) \propto r^{-\alpha} \qquad (0 < \alpha < 2). \tag{25}$$

This produces a potential, $\phi(r)$, that is finite at the center and satisfies

$$\phi(r) - \phi(0) \propto r^{2-\alpha}. \tag{26}$$

If we assume that the velocity distribution is isotropic (this is not a bad assumption near the center), we find that the density distribution (25) corresponds to the distribution function

$$f(E) \propto [E - \phi(0)]^{-(6-\alpha)/2(2-\alpha)}. \tag{27}$$

Thus, f diverges as $E \to \phi(0)$. This divergence causes difficulty in numerical integration of the FP equation, and therefore we had to stop our calculations at relatively early (low central density) collapse phases for the models with mass stripping. The depth of the central potential well becomes shallower as α decreases (Tremaine et al. 1994).

As is argued by Tremaine et al. (1994), the dependence of the velocity dispersion, $v_{\rm m}^2$, on the radius for the density cusp represented by equation (25) changes at $\alpha = 1$. We find

$$v_{\rm m}^2(r) \propto r^{2-\alpha}, \qquad \text{for } \alpha > 1, \tag{28}$$

which is the equation expected from a dimensional analysis. For $\alpha < 1$, the behavior of the velocity distribution is more subtle, since it is dominated by high-energy parts of the distribution function, which must deviate from equation (27) if the total mass is to be finite. If we consider any finite-mass model, we find

$$v_{\rm m}^2(r) \propto r^{\alpha} \qquad \text{for } \alpha < 1 \tag{29}$$

(see also Dehnen 1993). For any $\alpha < 2$, $v_{\rm m}^2 \to 0$ as $r \to 0$, and hence cool core collapse is expected.

In figure 11 we plot the evolution of the central densities and the central velocity dispersions of the galaxy and common halo components for models FPA1 and FPC1. Here the velocity dispersion of the galaxies is the mass-weighted average over all the galaxies. The central density increases with time in both models, but the behavior of the velocity dispersion is very different between FPA1 and FPC1. As we expected, the central velocity dispersion of the galaxies does decrease as core collapse proceeds in model FPC1, while it increases in model FPA1. In model

FPC1, even the central velocity dispersion of the common halo finally decreases when core collapse accelerates. It is considered that this is because cool halo particles are being supplied from cool central galaxies. (Remember we assumed that the particles stripped from a galaxy initially have the same energy and angular momentum per unit mass as those of its parent galaxy.)

We now consider why the velocity dispersion of the galaxies continue to decrease when mass stripping is included. Spitzer (1969) showed that equipartition among different mass components cannot be achieved if self-gravity of heavy components is strong. It is instructive to recall here his simple model. Consider a spherical system composed of particles of two different masses, m_1 and m_2 ($m_1 < m_2$). We assume that the total mass of the light component is much larger than that of the heavy component, $M_1 \gg M_2$, and that the heavy component is concentrated at the center. Then, the virial theorem for component 2 can be written as

$$v_2^2 = a\frac{GM_2}{R_2} + b\frac{GM_1R_2^2}{R_1^3}, \tag{30}$$

where v_2 is the mean velocity dispersion for component 2, R_1 and R_2 are the median radii of components 1 and 2, respectively, and a and b are numerical constants. *For fixed M_1, M_2, and R_1,* the right side has a minimum value of

$$v_{2,\min}^2 = 2(a^2b)^{1/3}\frac{G(M_1M_2^2)^{1/3}}{R_1} \tag{31}$$

at $R_2 = R_{2,\rm crit} \equiv (aM_2/bM_1)^{1/3}R_1$. The minimum of v_2^2 exists because the heavy particles form a self-gravitating system by themselves when $R_2 \ll R_{2,\rm crit}$, but behave as a non-self-gravitating system when $R_2 \gg R_{2,\rm crit}$. Therefore, after the concentration of the heavy component becomes sufficiently high, its velocity dispersion increases as the heavy component loses energy and contracts. However, if we now allow M_2 to change with $M_1 + M_2$ fixed, we find that $v_{2,\min}^2 \to 0$ and $R_{2,\rm crit} \to 0$ as $M_2 \to 0$. This implies that the velocity dispersion of the heavy component can continue to decrease to zero as the core shrinks, if mass stripping proceeds at an appropriate speed. Mass stripping prevents the heavy component from forming an independent self-gravitating system.

We may expect that core collapse changes its nature from cool collapse to hot collapse as tidal stripping becomes less and less important compared with two-body relaxation. To confirm this, we ran models FPC7, C8, and C9, which are the same as model FPC1 but have $C = 2.5$, 0.25, and 0.025, respectively. In principle, we should change the initial models of galaxies and clusters rather than C, which is considered to be roughly constant, in order to see the evolution of clusters with different stripping importance. From equation (20) we find that stripping becomes less important as $v_{\rm g0}/V_{\rm cl}$ increases with the other parameters fixed. Thus, very low stripping rates imply the condition $v_{\rm g0} \gg V_{\rm cl}$. (cf. In star clusters the escape velocity from a star is much larger than the velocity dispersion of stars.) However, we should not directly apply the equations for tidal stripping presented in subsections 2.2 and 2.3 to such cases, since those equations are considered to be valid only for $V_{\rm cl} \gtrsim v_{\rm g0}$. We therefore choose to change C just to conveniently control the stripping efficiency in our theoretical experiments.

Figure 12 shows the growth of the common halo mass for models FPC1 and FPC7–C9. It is interesting that the difference in the growth rates at the late times is within an order of magnitude among these models ($[T_{\rm cr}/M_{\rm cl}][dM_{\rm h}/dt] \sim 0.03$, 0.08, 0.05, and 0.01 for FPC1, C7, C8, and C9, respectively), while C varies over three orders of magnitude. This may be explained by a kind of self-regulation mechanism: if C is large, the galaxies quickly become more compact through initial violent stripping, and then the stripping speed slows down; if C is small, the central density can increase to very high values, and this finally increases the stripping rate at the central regions.

Figure 13 shows the evolution of the central density and velocity dispersion of the galaxy component for models FPC1 and FPC7–C9. The transition from cool collapse to hot collapse occurs at $C \sim 0.25$. In model FPC8 the central velocity dispersion increases until the central density increases by about a factor of 10^3, but decreases after that. Equation (20) tells us that in the present models the stripping time eventually becomes shorter than the relaxation time as $V_{\rm cl}$ increases toward infinity. Thus, we expect that for any small value of C, tidal stripping will become effective and the velocity dispersion will begin to decrease when the velocity dispersion has increased to a critical value, which is inversely proportional to C. The above results show that, unless the stripping rate is decreased to a very low value compared to the standard value, cool collapse occurs. Therefore, under the conditions of real galaxy clusters ($V_{\rm cl} \gg v_{\rm g0}$), cool collapse is expected to occur.

Figures 14 shows the profiles of the density and the logarithmic density gradient α for model FPC7 ($C = 2.5$), and figure 15 shows those for model FPC9 ($C = 0.025$). In model FPC7 a shallow density cusp of $\alpha < 2$ develops, but this cusp is steeper than the cusp in model FPC1 (see figure 8). In model FPC9 a deep cusp of $\alpha > 2$ develops, and α approaches 2.2 as the core collapse proceeds. Unlike in no-stripping models FPA, the central density of the halo component also significantly rises in model FPC9 due to continuous production of new halo particles.

Figures 16a and b show the evolution of velocity dispersion profiles for models FPC7 and FPC9, respectively. In these figures qualitative difference between models FPC7 and FPC9 is clearly seen. In model FPC7 an inverse velocity dispersion gradient develops in the central regions.

7. Summary and Discussion

In this study, we investigated the dynamical evolution of galaxy clusters after virialization using FP models and compared these models with the N-body models of SFM99 and SFM00. Our FP models included the effects of gravitational two-body encounters between galaxies and between galaxies and common halo particles which are much lighter than the galaxies. Furthermore, tidal stripping of mass from the galaxies to the common halo and accompanying dissipation of the orbital kinetic energies of the galaxies were included using revised cross-section formulae.

We found that the results of the FP models agree very well with those of the N-body models regarding the growth of the common halo mass and the evolution of the cluster density profiles. This indicates that all of the important physical processes that occur in the N-body models are properly included in the FP models. Although there is some ambiguity in the cross sections of mass stripping and energy dissipation, we found that the results of the FP simulations do not sensitively depend on the details of the cross-section formulae.

In the evolution of galaxy clusters, tidal mass stripping from galaxies is very important. Under the initial conditions that SFM99 and SFM00 employed, where the total cluster mass is initially attached to galaxies, more than half of the total mass turns into the common halo during a first few crossing times. Heavy galaxies sink toward the cluster center owing to dynamical friction. However, a high density of galaxies results in strong stripping, and thus it is usually seen in our models that the mean mass of galaxies decreases toward the center, which is inverse mass segregation. Dissipation of the orbital kinetic energies of galaxies due to tidal stripping also plays an important role in accelerating the sinking of the galaxies toward the cluster center, if the velocity dispersion of the stars in the galaxies is not very small compared to that of the galaxies in the cluster.

As the central density increases, a cusp profile, approximated by a power law, $\rho \propto r^{-\alpha}$, develops at the core region. In the model clusters of SFM99 and SFM00, α for the total density is $\sim$1. This density distribution consists of the galaxy component with larger α (still < 2) and the common halo component with smaller α. The development of the density cusp is a consequence of the collisional evolution of galaxy clusters.

The slope of the density cusp, α, depends on the ratio of the stripping rate to the relaxation rate. When the effect of stripping is negligible compared to relaxation, "hot core collapse", which is usual gravothermal collapse, occurs: i.e., as the core shrinks both the central density and velocity dispersion increase, and a deep cusp with $\alpha \sim 2.2 > 2$ develops. When stripping is important, "cool core collapse" occurs: while the central density increases, the central velocity dispersion decreases, and consequently a shallow cusp ($\alpha < 2$) develops. Faster tidal stripping results in shallower cusps. Under the conditions of real galaxy clusters, tidal stripping is rather effective and cool collapse is expected to occur.

One might think that this conclusion is in contradiction with the results of SFM00, who showed using N-body simulations that the profile with $\alpha \sim 1.2$ (1–1.5) develops regardless of the initial models of galaxies and clusters. Actually, their results are consistent with the results of this paper. SFM00 varied the initial models of galaxies and clusters adopting Plummer, King (King 1966), and Hernquist models (Hernquist 1990), but did not vary the number of galaxies and the ratio of the galaxy virial radius to the cluster virial radius. As a result, the growth rates of the common halo mass, or the mean stripping rates are similar among all of their runs. Our FP simulations show that while α depends on the stripping rate, it does so only weakly. Therefore, it is no wonder that no significant difference in α has been detected among the N-body models of SFM00.

Hot core collapse terminates with the formation of hard binaries. Because of subsequent energy release from these binaries, the core starts to expand (see, e.g., Spitzer 1987). What is the end state of cool collapse? Through cool collapse, low-energy galaxies accumulate around the cluster center. They finally merge and form a massive central galaxy. The central galaxy will further grow by eating galaxies falling to the center in succession, and this process will continue until all galaxies, except for the central one, disappear. Thus, we will see at last one giant (cD ?) galaxy with an enormous halo. In the present study we did not include the merging process in FP models, and hence we could not follow very late stages of the cluster evolution with FP models. Future N-body calculations as well as improved FP models will reveal the consequences of cool collapse in more detail.

This work was supported in part by the Research for the Future Program of Japan Society for the Promotion of Science (JSPS-RFTP97P01102).

References

Athanassoula, E., Bosma, A., Lambert, J.-C., & Makino, J. 1998, MNRAS, 293, 369
Bahcall, J. N., & Wolf, R. A. 1977, ApJ, 216, 883
Barnes, J. E., & Hut, P. 1986, Nature, 324, 446
Bode, P. W., Berrington, R. C., Cohn, H. N., & Lugger, P. M. 1994, ApJ, 433, 479
Casertano, S., & Hut, P. 1985, ApJ, 298, 80
Chernoff, D. F., & Weinberg, M. D. 1990, ApJ, 351, 121
Cohn, H. 1979, ApJ, 234, 1036
Cohn, H. 1980, ApJ, 242, 765
Cohn, H. 1985, in Dynamics of Star Clusters, IAU Symp No.113, ed J. Goodman, P. Hut (Dordrecht: D. Reidel Publishing Company) p161
Dehnen, W. 1993, MNRAS, 265, 250

Table 1. Fokker–Planck models.

Model	η_v	η_m	ζ	C	Note
FPA1	⋯	⋯	⋯	0	$M_{\rm h}/M_{\rm cl}=1/2$
FPA2	⋯	⋯	⋯	0	$M_{\rm h}/M_{\rm cl}=3/4$
FPB1	2	2	1/4	25	No dissipation
FPC1	2	2	1/4	25	Standard model
FPC2	2	2	1/4	15	
FPC3	2	2	1/4	35	
FPC4	3	2	1/4	100	
FPC5	2	1	1/4	25	
FPC6	2	2	1/3	25	
FPC7	2	2	1/4	2.5	
FPC8	2	2	1/4	0.25	
FPC9	2	2	1/4	0.025	

Ferguson, H. C., Tanvir, N. R., & von Hippel, T. 1998, Nature, 391, 461

Funato, Y., & Makino J. 1999, ApJ, 511, 625 (FM)

Funato, Y., Makino, J., & Ebisuzaki, T. 1993, PASJ, 45, 289

García-Gómez, C., Athanassoula, E., & Garijo, A. 1996, A&A, 313, 363

Garijo, A., Athanassoula, A., & García-Gómez, C. 1997, A&A, 327, 930

Heggie, D. C., & Mathieu, R. D. 1986, in The Use of Supercomputers in Stellar Dynamics, ed P. Hut, S. McMillan (Berlin: Springer) p233

Hernquist, L. 1990, ApJ, 356, 359

Inagaki, S., & Wiyanto, P. 1984, PASJ, 36, 391

King, I. 1966, AJ, 71, 64

Lee, H. M. 1987, ApJ, 319, 801

Lynden-Bell, D., & Eggleton, P. P. 1980, MNRAS, 191, 483

Lynden-Bell, D., & Wood R. 1968, MNRAS, 138, 495

Makino, J. 1991, PASJ, 43, 621

Makino, J., Taiji, M., Ebisuzaki, T., & Sugimoto, D. 1997, ApJ, 480, 432

Merritt, D. 1983, ApJ, 264, 24

Merritt, D. 1984, ApJ, 276, 26

Merritt, D. 1985, ApJ, 289, 18

Quinlan, G. D., & Shapiro, S. L. 1989, ApJ, 343, 725

Scheick, X., & Kuhn, J. R. 1994, ApJ, 423, 566

Sensui, T., Funato, Y., & Makino, J. 1999, PASJ, 51, 943 (SFM99)

Sensui, T., Funato, Y., & Makino, J. 2000, PASJ, submitted (astro-ph/0012092) (SFM00)

Spitzer, L., Jr. 1969, ApJ, 158, L139

Spitzer, L., Jr. 1987, Dynamical Evolution of Globular Clusters (Princeton: Princeton University Press)

Takahashi, K. 1995, PASJ, 47, 561

Takahashi, K. 1997, PASJ, 49, 547

Tremaine, S., Richstone, D. O., Byun, Y.-I., Dressler, A., Faber, S. M., Grillmair, C., Kormendy, J., & Lauer, T. R. 1994, AJ, 107, 634

Vílchez-Gómez, R., Pelló, R., & Sanahuja, B. 1994, A&A, 283, 37

Yepes, G., & Domínguez-Tenreiro, R. 1992, ApJ, 387, 27

Yepes, G., Domínguez-Tenreiro, R., & del Pozo-Sanz, R. 1991, ApJ, 373, 336

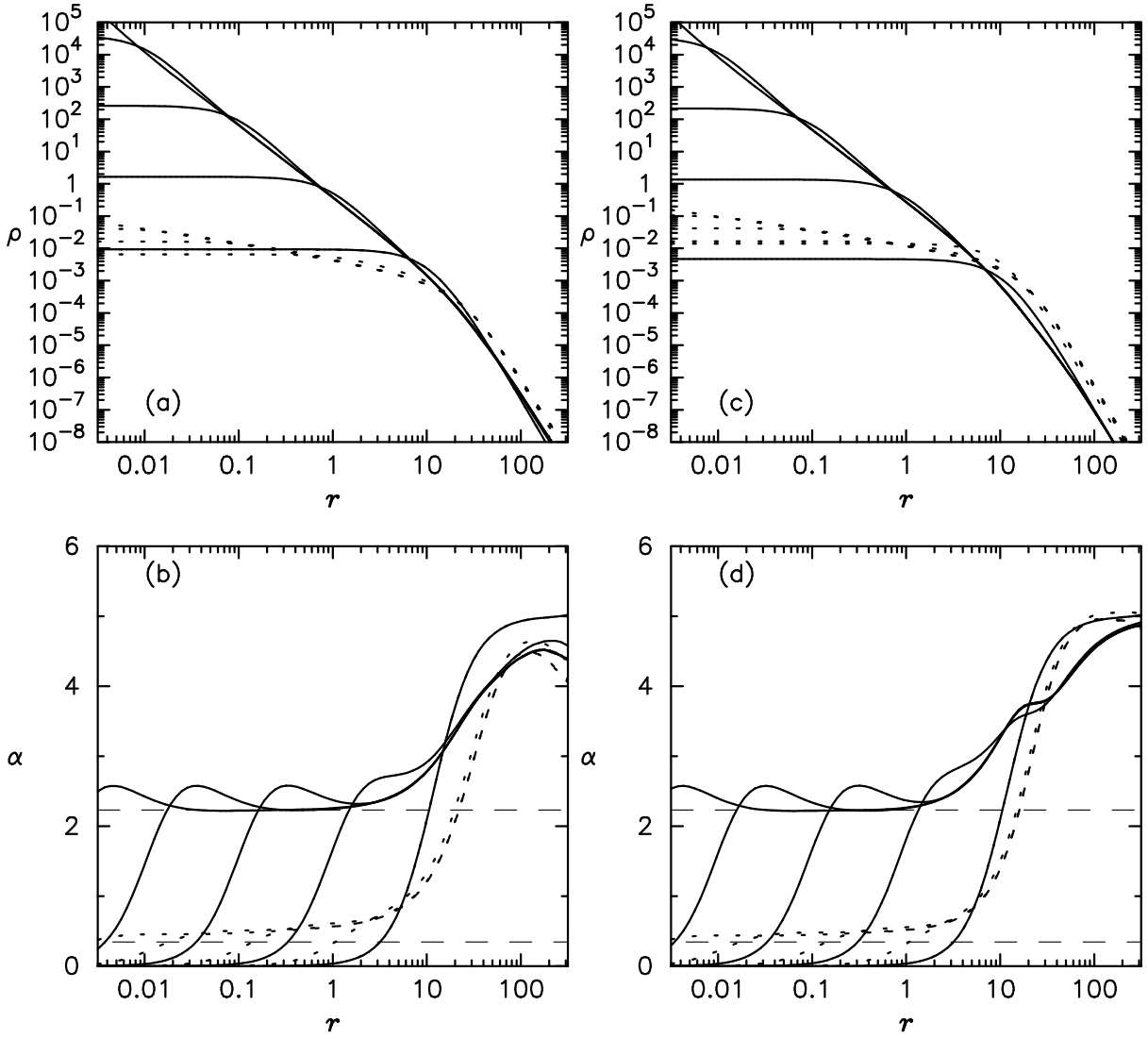

Fig. 1. (a) Evolution of the density profiles of the galaxy component (solid) and common halo component (dotted) for model FPA1. Plotted are the profiles at $t/T_{\rm cr} = 0$, 6.7, 7.99, 8.0209, 8.0214. The central densities of both components increase with time, except that the central density of the halo component decreases initially. (b) The logarithmic density gradient $\alpha \equiv -d\ln\rho/d\ln r$ for the density profiles shown in (a). The two horizontal dashed lines are $\alpha = 2.23$ and $\alpha = 0.345$ (see text). (c) Same as (a), but for model FPA2. Plotted are the profiles at $t/T_{\rm cr} = 0$, 4.5, 5.42, 5.4454, 5.4457. The central densities of both components increase with time. (d) Same as (b), but for model FPA2.

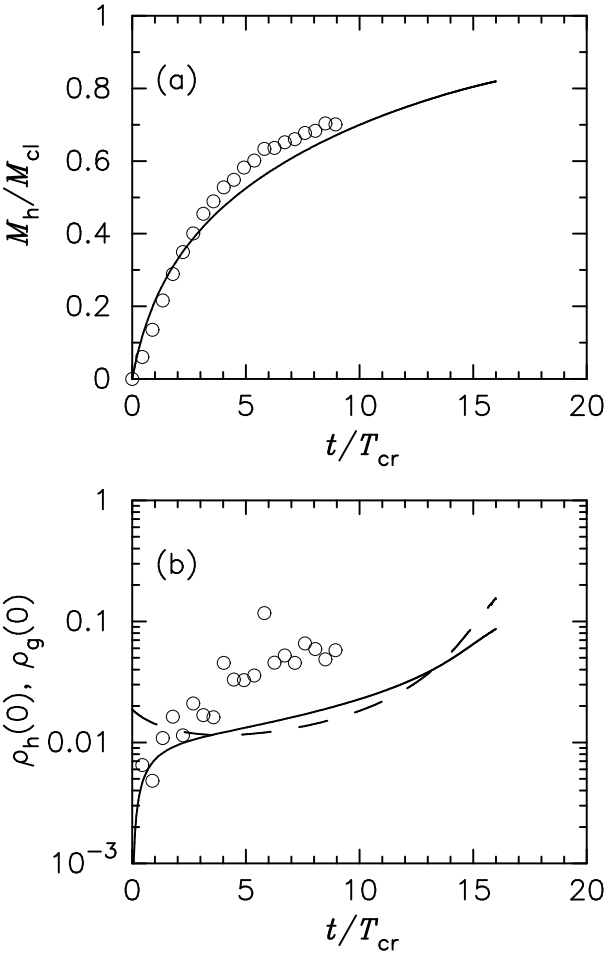

Fig. 2. (a) Ratio of the common halo mass, $M_{\rm h}$, to the total cluster mass, $M_{\rm cl}$, as a function of time. The circles represent model NB and the solid line represents model FPB1. (b) Evolution of the central density of the common halo component (solid) and that of the galaxy component (dashed) for model FPB1. The circles represent the central density of the common halo for model NB.

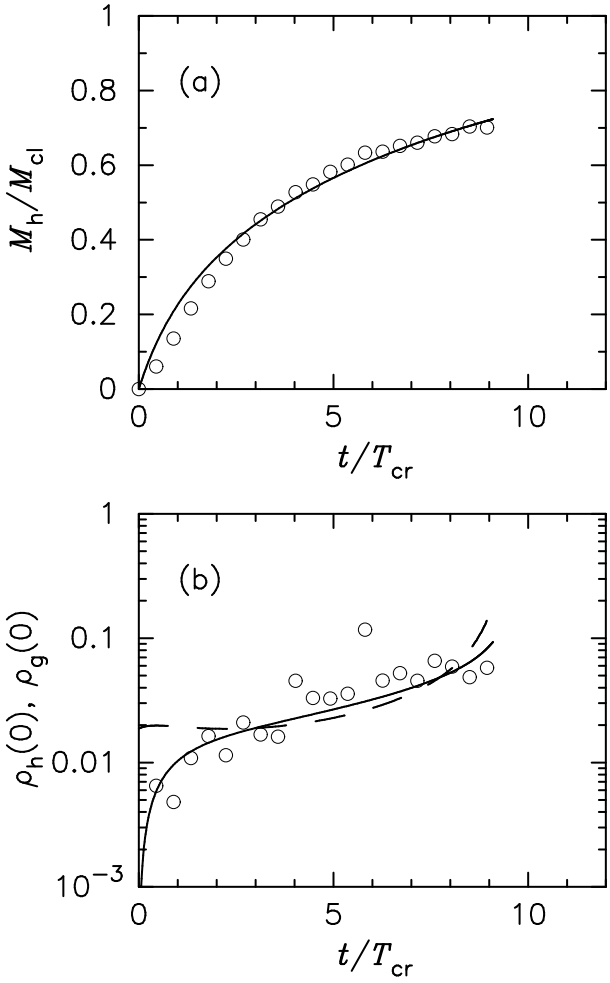

Fig. 3. Same as figure 2, but model FPC1 is compared with model NB.

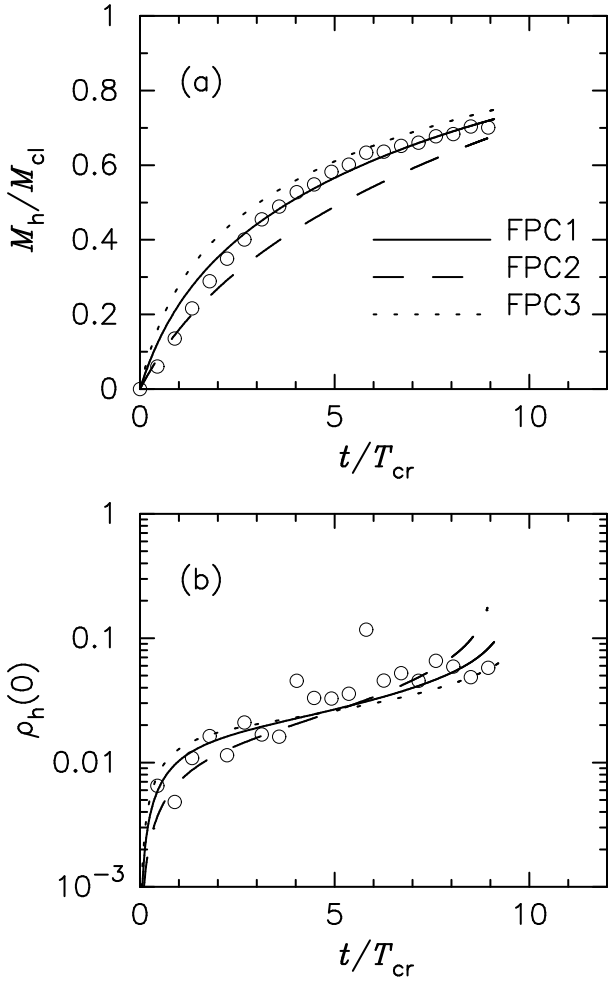

Fig. 4. Same as figure 2, but the results for models FPC1, FPC2, and FPC3 are shown by the solid, dashed, and dotted lines, respectively. In (b) only the central density of the common halo is shown.

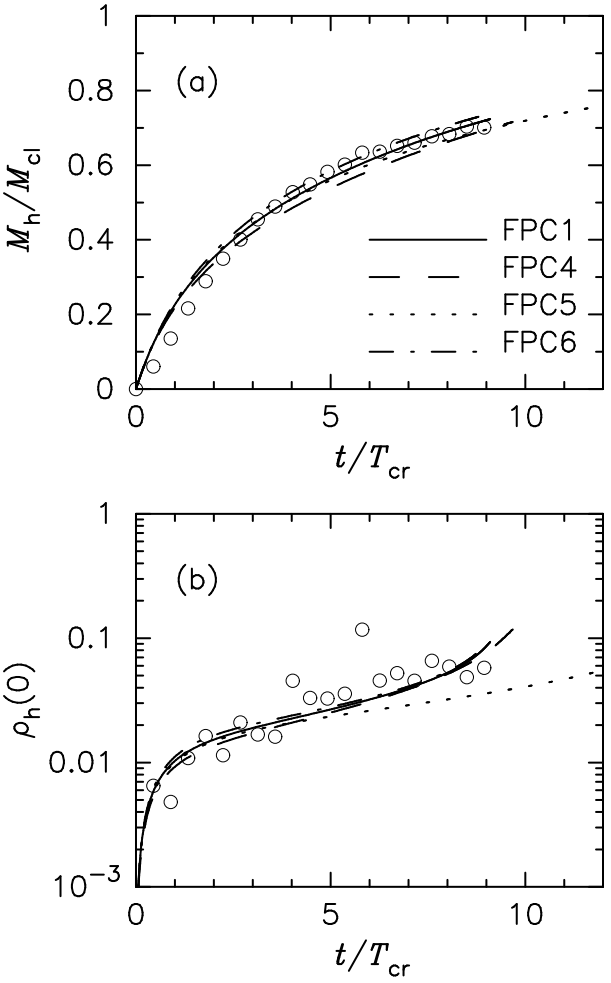

Fig. 5. Same as figure 4, but the results for models FPC1, FPC4, FPC5, and FPC6 are shown by the solid, dashed, dotted, and dash-dotted lines, respectively.

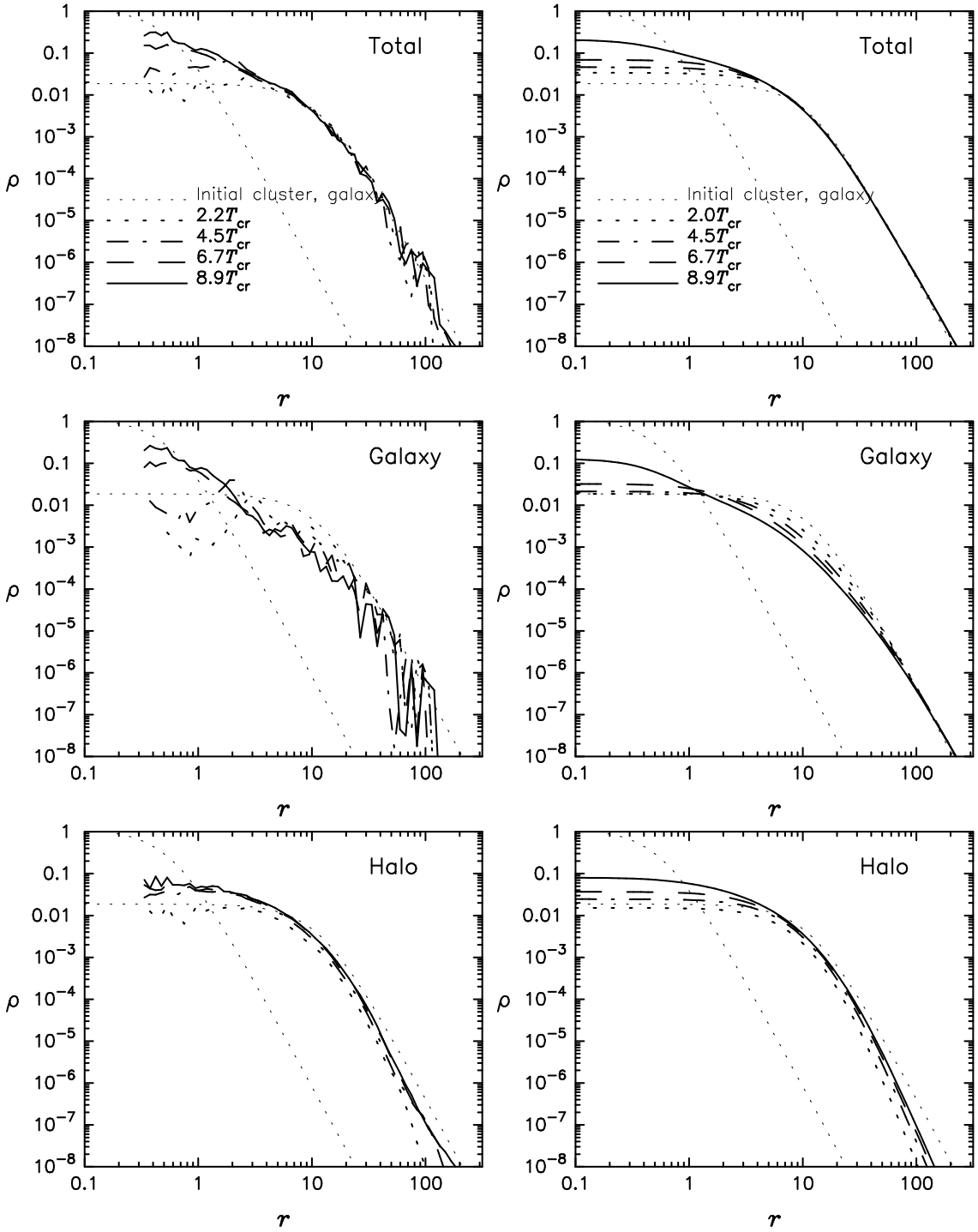

Fig. 6. Density profiles of models NB (left) and FPC1 (right) at selected epochs. The top panels show the total density, and the middle and bottom panels show the densities of the galaxy component and the common halo component, respectively. The density profile of the initial cluster as well as the profile of an initial galaxy (here its center is placed at the cluster center) is plotted with thin dotted lines.

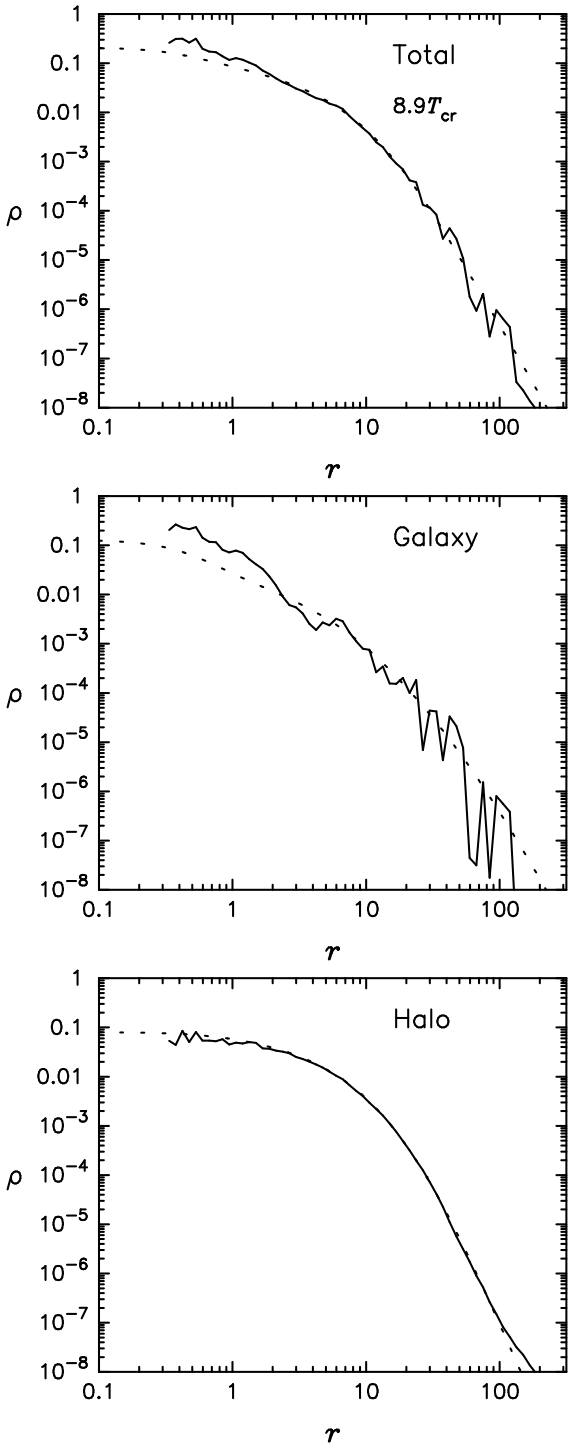

Fig. 7. Comparison of the density profiles of models NB (solid) and FPC1 (dotted) at $t = 8.9T_{\rm cr}$. The top panel shows the total density, and the middle and bottom panels show the densities of the galaxy component and the common halo component, respectively. Note that the two models should be compared with caution for $r \lesssim 1$, because in model NB the galaxies have sizes of ~ 1 and their internal structure is seen on the scale of $r \lesssim 1$.

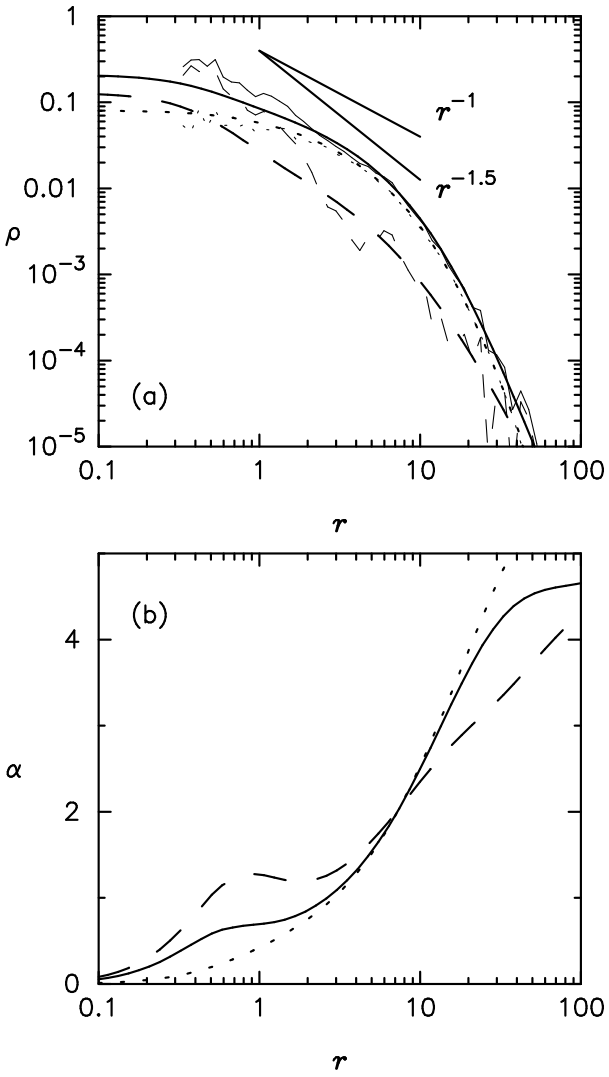

Fig. 8. (a) Density profile $\rho(r)$ for model FPC1 at $t = 8.9T_{\rm cr}$. The solid, dashed, and dotted lines represent the total density, the galaxy component, and the common halo component, respectively. The density profiles for model NB at $t = 8.9T_{\rm cr}$ are also shown by thin lines. (b) Logarithmic density gradient, $\alpha(r) \equiv -d\ln\rho/d\ln r$, corresponding to the density profiles for model FPC1 shown in panel (a).

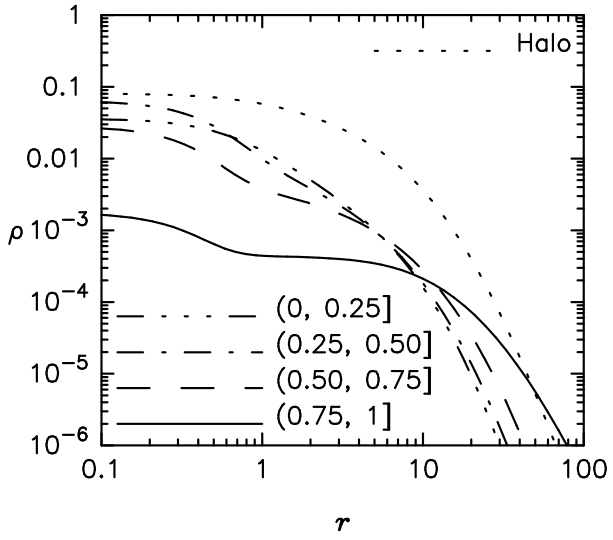

Fig. 9. Density profiles for the galaxies in four mass ranges, $(0, 0.25]$, $(0.25, 0.50]$, $(0.50, 0.75]$, and $(0.75, 1]$, separately shown for model FPC1 at $t = 8.9T_{\rm cr}$. The dotted line is for the common halo.

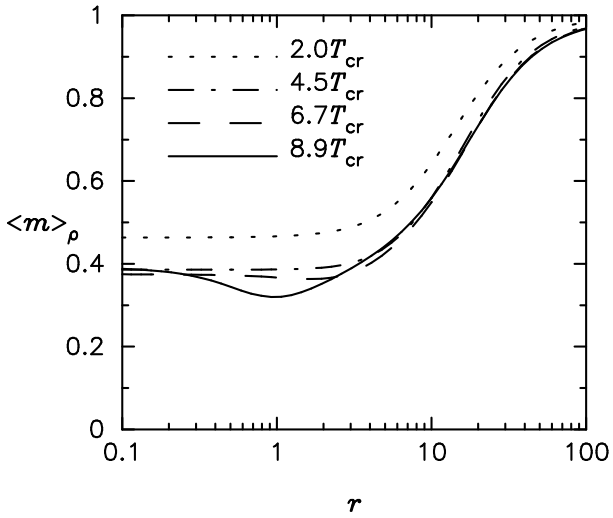

Fig. 10. Mean galaxy mass $\langle m \rangle_\rho$ as a function of radius for model FPC1 at selected epochs.

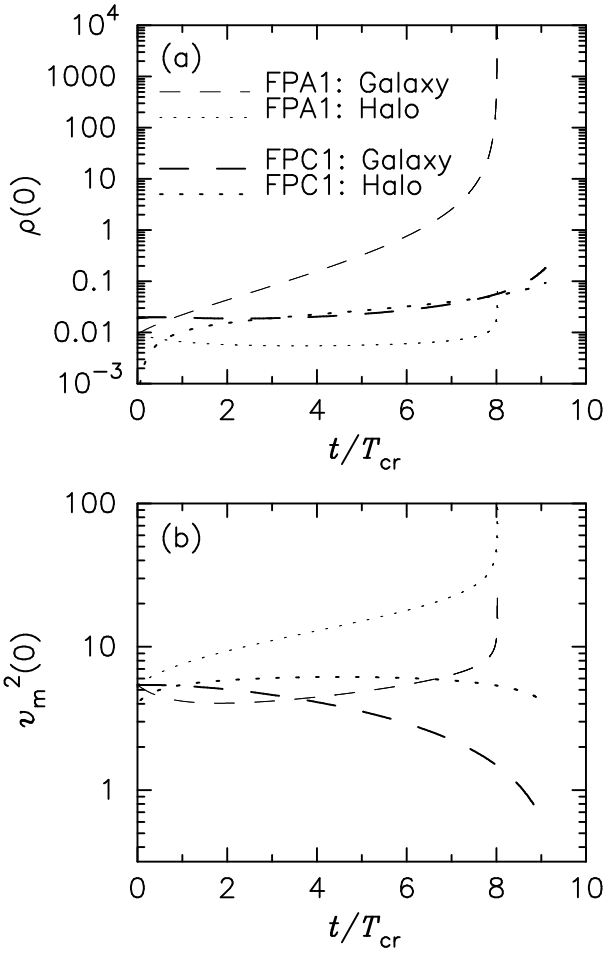

Fig. 11. (a) Evolution of the central densities of the galaxy component (dashed) and the halo component (dotted) for models FPA1 and FPC1. (b) Evolution of the central velocity dispersions of the galaxy component (dashed) and the halo component (dotted) for models FPA1 and FPC1.

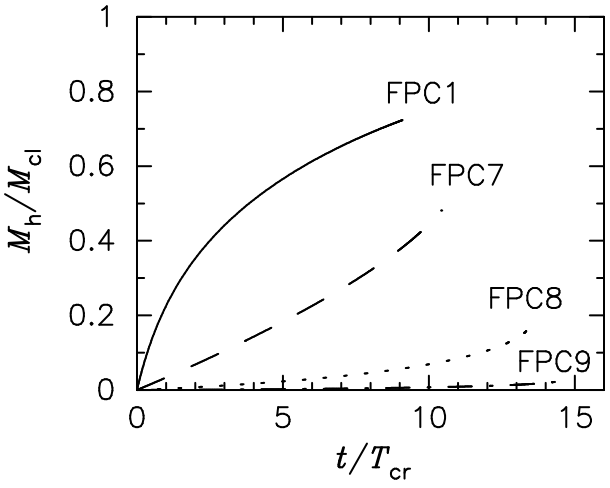

Fig. 12. Growth of the common halo mass for models FPC1, FPC7, FPC8, and FPC9.

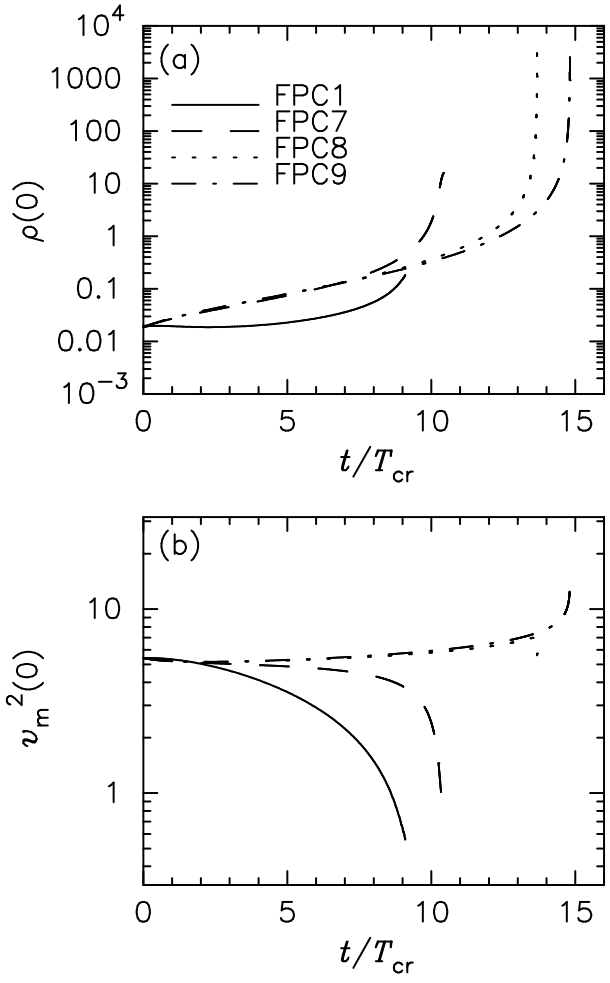

Fig. 13. (a) Evolution of the central density of the galaxy component for models FPC1, FPC7, FPC8, and FPC9. (b) Evolution of the central velocity dispersion of the galaxy component for models FPC1, FPC7, FPC8, and FPC9.

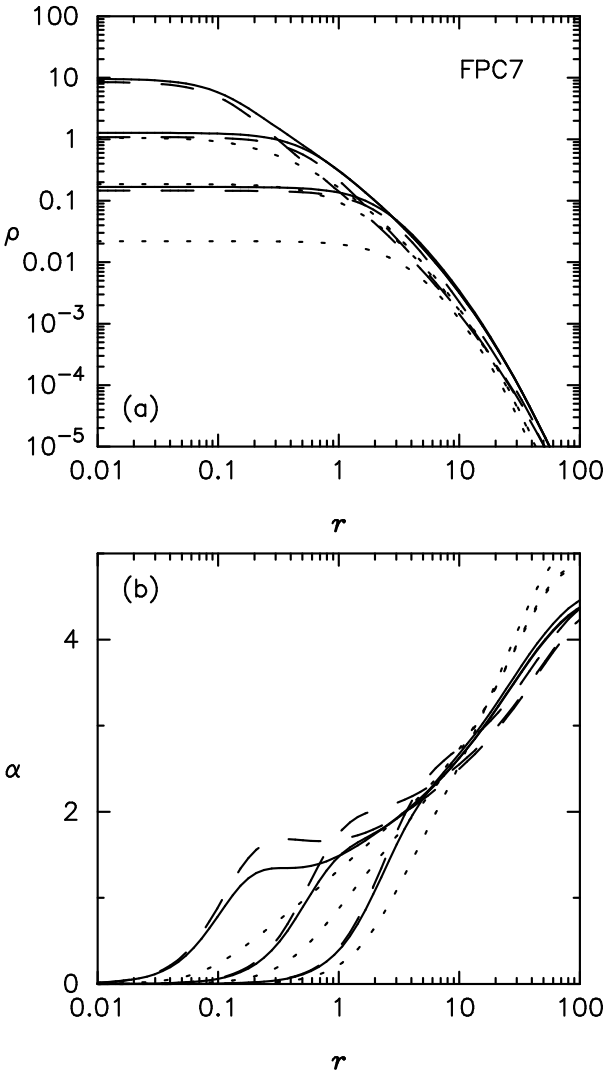

Fig. 14. (a) Evolution of the density profile for model FPC7. The profiles at $t/T_{\rm cr} = 7.1$, 9.8, and 10.3 are plotted. The solid, dashed, and dotted lines represent the total density, the galaxy component, and the common halo component, respectively. (b) The profiles of the logarithmic density gradient, α, corresponding to the density profiles shown in panel (a).

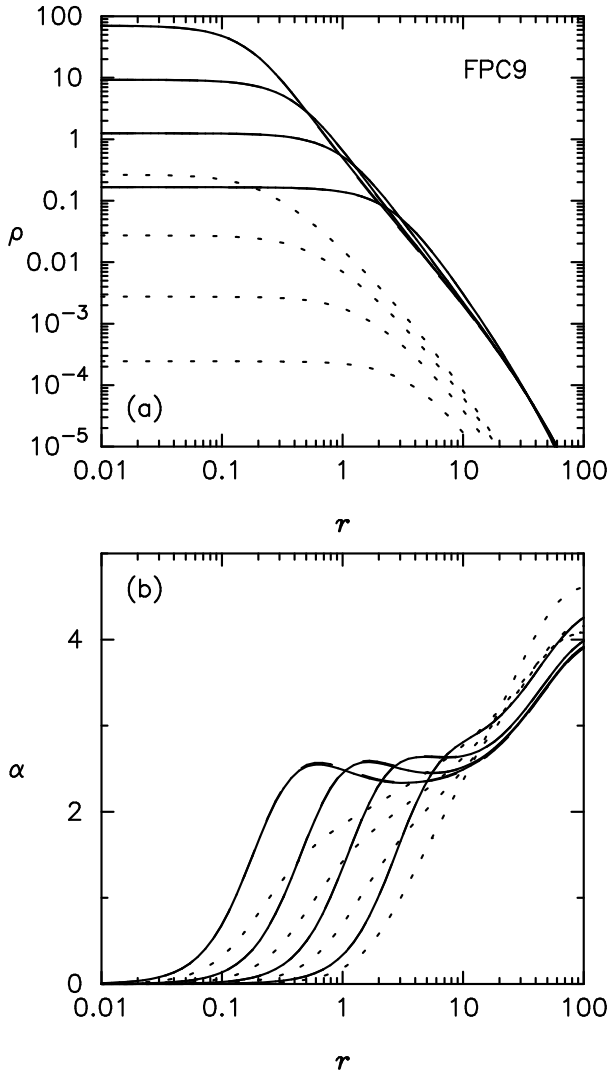

Fig. 15. Same as figure 14, but for model FPC9. The profiles at $t/T_{\rm cr} = 7.8$, 12.7, 14.3, and 14.7 are plotted.

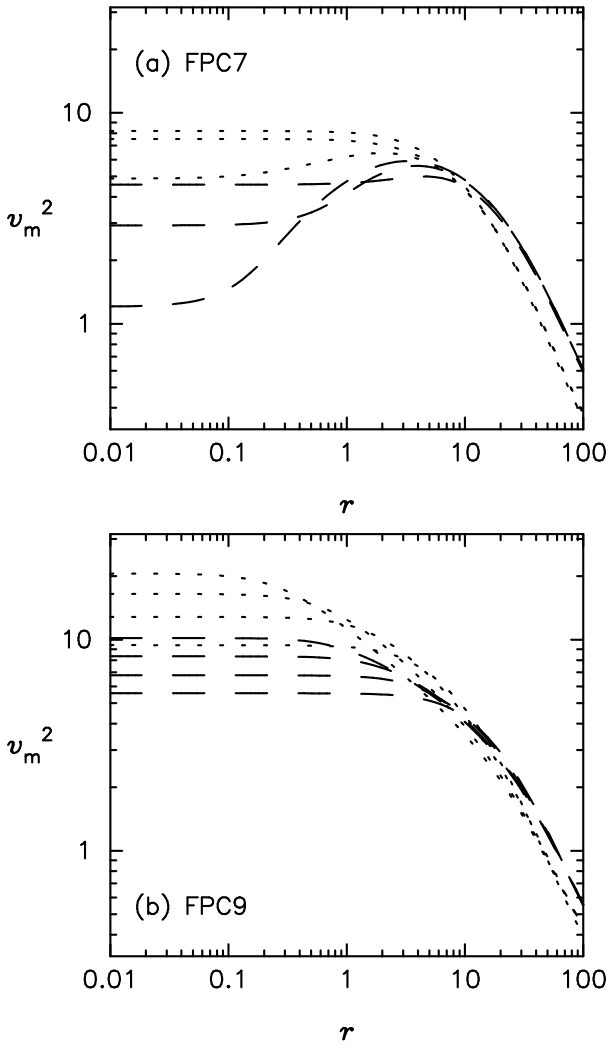

Fig. 16. (a) Evolution of the velocity dispersion profiles for model FPC7. The profiles at the same epochs as in figure 14 are plotted. The dashed and dotted lines represent the galaxy and common halo components, respectively. For the galaxy the mass-weighted mean velocity dispersion is plotted. The central velocity dispersions of both components decrease with time. (b) Same as (a), but for model FPC9. The profiles at the same epochs as in figure 15 are plotted. The central velocity dispersions of both components increase with time.